Integral Boundary Layer Formulation for Blunt Trailing Edges

89-2166-CP

Mark Drela†
Computational Fluid Dynamics Laboratory, Department of Aeronautics and Astronautics
Massachusetts Institute of Technology

Abstract

Extensions to a two-equation lag-dissipation closure integral boundary layer formulation are developed. The wake is treated as one viscous layer which is matched to the upper and lower airfoil surface boundary layers at the trailing edge. A special treatment of the near wake behind a blunt trailing edge is employed, consisting of a correction to the shape parameter correlation to account for the highly irregular velocity profile in the near wake. The momentum and displacement thickness distributions on the airfoil surfaces and wake compare very well with experiment for transonic and high subsonic flows. The rapid momentum thickness rise immediately behind the blunt trailing edge, representing "base drag", is captured particularly well, giving the correct far downstream momentum thickness and hence an accurate overall drag prediction. Further work is necessary to more accurately predict mean trailing edge flows with periodic vortex shedding.

Nomenclature

c	airfoil chord
C_D	dissipation coefficient $= \frac{1}{\rho_e u_e^3} \int \tau \frac{\partial u}{\partial \eta} \, d\eta$
C_f	skin friction coefficient $= \frac{2\tau_{wall}}{\rho_e u_e^2}$
C_τ	shear stress coefficient $= \frac{\tau_{max}}{\rho_e u_e^2}$
h_{TE}	trailing edge thickness
H	shape parameter $= \frac{\delta^*}{\theta}$
H^*	kinetic energy shape parameter $= \frac{\theta^*}{\theta}$
H^{**}	density shape parameter $= \frac{\delta^{**}}{\theta}$
H_k	kinematic shape parameter $= \int \left(1 - \frac{u}{u_e}\right) d\eta \Big/ \int \frac{u}{u_e}\left(1 - \frac{u}{u_e}\right) d\eta$
M_e	boundary layer edge Mach number
Re_θ	momentum thickness Reynolds number $= \frac{\rho_e u_e \theta}{\mu_e}$
u_e	boundary layer edge velocity
u_S	effective outer layer slip velocity
u_τ	wall shear velocity $= \sqrt{\frac{\tau_{wall}}{\rho}}$
x	Cartesian x-coordinate
δ	boundary layer thickness
δ^*	displacement thickness $= \int \left(1 - \frac{\rho u}{\rho_e u_e}\right) d\eta$
δ^{**}	density thickness $= \int \frac{u}{u_e}\left(1 - \frac{\rho}{\rho_e}\right) d\eta$
ξ, η	thin shear layer coordinates
θ	momentum thickness $= \int \frac{\rho u}{\rho_e u_e}\left(1 - \frac{u}{u_e}\right) d\eta$
θ^*	kinetic energy thickness $= \int \frac{\rho u}{\rho_e u_e}\left(1 - \frac{u^2}{u_e^2}\right) d\eta$
μ_e	boundary layer edge viscosity
ρ	density
ρ_e	boundary layer edge density
τ	shear stress

1 Introduction

The viscous model in the original coupled viscous/inviscid ISES code [1] is an integral, two-equation dissipation closure formulation with lag effects in the turbulent stresses. The inviscid Euler formulation and integral viscous formulation are coupled through the displacement thickness and solved simultaneously with a global Newton method. This code has given excellent results for a very wide range of airfoil and cascade applications, including low Reynolds number and shocked transonic cases [2], [3]. Following Green et al [4], the original ISES code treats the turbulent wake as two distinct boundary layers with zero skin friction, which has proven to be a realistic and accurate model for sharp trailing edges, even with the substantial near-wake assymetry typical on lifting airfoils. Blunt trailing edges are treated by the incorporation of a short flap which extends from the trailing edge several base thicknesses downstream. The flap has a prescribed thickness ending with a cusp, and is free to move up and down so that it carries no load. The inviscid flow sees the flap thickness plus the total displacement thickness of the upper and lower wake halves. This produces a smooth displacement body over the trailing edge region.

The accuracy of this formulation for blunt trailing edges has never been firmly established due to the lack of sufficiently detailed and reliable experimental data. Airfoils with relatively blunt trailing edges are quite frequently employed whenever dictated by severe structural requirements, particularly in helicopter rotors and turbomachinery. It is of great practical interest to be able to accurately predict the profile drag penalty or "base drag" of a blunt airfoil trailing edge, so that a more optimal structural-aerodynamic compromise can be struck before an expensive committment to hardware is made.

Cook and McDonald [5] have relatively recently presented high-quality measurements in the near wake behind an airfoil with a 1.14% trailing edge base thickness. Calculations with the original ISES code revealed some deficiencies in the calculated results, with the drag increase due to the blunt trailing edge being underpredicted. Figure 1 shows the old calculated C_p distributions for Case 1 compared against measurements, and Figure 2 shows the corresponding δ^* and θ distributions. Although the C_p distribution is reasonably well predicted, the θ jump just behind the trailing edge is significantly underpredicted, which leads to the underpredicted overall drag, since the drag is taken directly from the far downstream value of θ as in a real wake traverse measurement.

The remainder of this paper presents changes to the integral dissipation closure formulation which have been made to more accurately model the wake development in the region immediately behind a blunt trailing edge. The changes should be applicable to any two-equation integral method, including those based on entrainment closure.

2 Boundary Layer Formulation

2.1 Governing Equations and Closure

The original and new formulations both employ the following standard integral momentum and kinetic energy

† Carl Richard Souderton Assistant Professor of Power Engineering, Member AIAA

Copyright © American Institute of Aeronautics and Astronautics, Inc., 1989. All rights reserved.

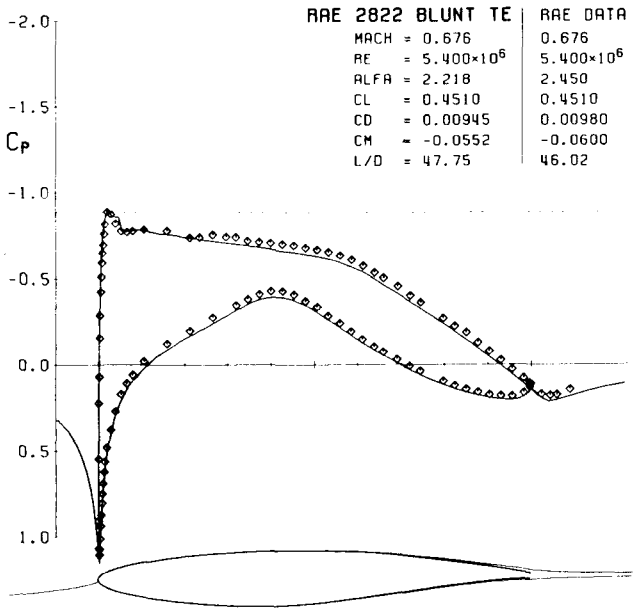

Figure 1: Calculated (line) and experimental (symbols) C_p vs x/c for Case 1. Old ISES wake formulation.

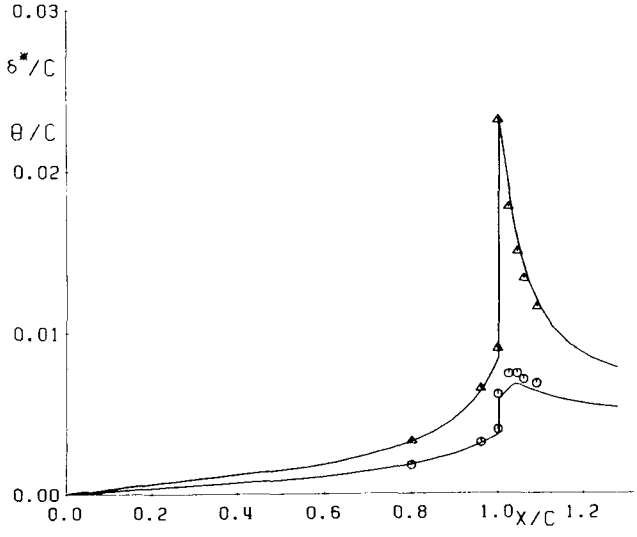

Figure 2: Calculated (line) and experimental (symbols) suction side and wake δ^* and θ vs x/c for Case 1. Old ISES wake formulation.

shape parameter equations.

$$\frac{d\theta}{d\xi} + (2 + H - M_e^2)\frac{\theta}{u_e}\frac{du_e}{d\xi} = \frac{C_f}{2} \tag{1}$$

$$\theta\frac{dH^*}{d\xi} + (2H^{**} + H^*(1-H))\frac{\theta}{u_e}\frac{du_e}{d\xi} = 2C_D - H^*\frac{C_f}{2} \tag{2}$$

Also, a rate equation for the maximum shear stress coefficient C_τ is used to account for lags in the response of outer layer Reynolds stresses to changing flow conditions.

$$\frac{\delta}{C_\tau}\frac{dC_\tau}{d\xi} = 4.2(C_{\tau_{EQ}}^{1/2} - C_\tau^{1/2}) \tag{3}$$

Equation (2) is readily derived by combining the standard integral momentum equation (1) and the kinetic energy thickness equation (4) below.

$$\frac{d\theta^*}{d\xi} + \left(\frac{\delta^{**}}{\theta^*} + 3 - M_e^2\right)\frac{\theta^*}{u_e}\frac{du_e}{d\xi} = 2C_D \tag{4}$$

The fundamental variables governed by these equations are chosen to be θ, δ^*, and C_τ. In addition, u_e is present as an external unknown which is related to the inviscid outer solution in the overall coupling scheme and is not treated as a boundary layer variable. To close the integral boundary layer equations (1), (2), and (3), auxilliary variables are defined in terms of θ, δ^*, C_τ, u_e or their suitable combinations with the following functional dependencies.

$$H_k = H_k(H, M_e) \tag{5}$$

$$H^* = H^*(H_k, M_e, Re_\theta) \tag{6}$$

$$H^{**} = H^{**}(H_k, M_e) \tag{7}$$

$$\delta = \delta(H_k, \theta, \delta^*) \tag{8}$$

$$U_S = U_S(H^*, H, H_k) \tag{9}$$

$$C_{\tau_{EQ}} = C_{\tau_{EQ}}(H^*, H, H_k, U_S) \tag{10}$$

$$C_f = C_f(H_k, M_e, Re_\theta) \tag{11}$$

The actual expressions for these correlations are given fully in Drela and Giles [2] and will not be repeated here. The non-dimensional effective slip velocity $U_S = u_S/u_e$ of the outer layer, and equilibrium shear stress coefficient $C_{\tau_{EQ}}$ are defined so that the method properly predicts the special case of equilibrium flows of Clauser [6] for which $C_\tau = C_{\tau_{EQ}}$. The rate equation (3) then determines the deviation of C_τ from $C_{\tau_{EQ}}$ in general non-equilibrium flows. The actual shear stress coefficient C_τ is used together with the slip velocity to define the outer layer contribution to the total dissipation coefficient C_D, with C_f and the slip velocity determining the inner layer contribution.

$$C_D = \frac{C_f}{2}U_S + C_\tau(1 - U_S) \tag{12}$$

2.2 Wake Closure Relations

The new viscous formulation treats the wake as one viscous layer instead of as two independent layers, so that only one θ and one δ^* variable is present at each wake station, and represents the total wake momentum and displacement thickness. Likewise, only one edge velocity u_e per wake station is required, and this is taken to be the average of the two velocities on each side of the wake. In strictly isentropic flow, these are the same since the pressure on each side of the wake is enforced to be the same. If shock waves are present on the airfoil, these velocities can differ somewhat. Treating the wake as one layer in this manner was made primarily for the sake of more realism, and the fact that only the total wake θ and δ^* can be rigorously defined. Robustness of the overall viscous/inviscid ISES algorithm has also noticably improved. If a separated laminar flow with a large shape parameter occurred at the start of the wake on one side at the trailing edge, the old half-wake formulation occasionally produced spurious behavior in that wake half far downstream.

The total wake quantities are governed by the same integral equations (1), (2) as the wall boundary layers. In addition, the rate equation (3) is assumed to remain valid as well, with the exception that the equilibrium shear stress coefficient $C_{\tau_{EQ}}$ is quadrupled from its wall boundary layer closure relation (10).

$$C_{\tau_{EQ}} = 4\, C_{\tau_{EQ}}(H^*, H, H_k, U_S) \qquad \text{(wake)} \qquad (13)$$

This accounts for the roughly quadrupled wake eddy viscosity compared to wall boundary layer levels, as observed by Green et al [4] from the data of Narasimha and Prabhu [7]. Also, the skin friction coefficient C_f in the wake is set to zero and the outer layer contribution to the dissipation coefficient C_D is doubled, with the inner layer contribution vanishing.

$$C_f = \; 0 \qquad \text{(wake)} \qquad (14)$$

$$C_D = \; 2\, C_\tau (1 - U_S) \qquad \text{(wake)} \qquad (15)$$

Doubling of the dissipation coefficient C_D is necessary because the outer layer term $C_\tau(1 - U_S)$ in the dissipation coefficient formula (12) pertains to a half-wake outer layer profile. A wake consists of two such profiles, each of which contributes roughly equally to the total dissipation. The quantities C_τ and U_S on which C_D depends in equation (12) do not convey this information.

2.3 Boundary Layer-Wake Matching

Special joining conditions are necessary at the trailing edge to fix the initial θ, δ^*, and C_τ values at the start of the wake. Examination of the measured velocity profiles tabulated in Cook and McDonald [5], reveals that the momentum thickness must be continuous, and the displacement thickness must have a jump equal to the trailing edge thickness h_{TE}.

$$\theta_{\text{wake}} = \theta_{\text{upper}} + \theta_{\text{lower}} \qquad (16)$$

$$\delta^*_{\text{wake}} = \delta^*_{\text{upper}} + \delta^*_{\text{lower}} + h_{TE} \qquad (17)$$

The initial wake shear coefficient is taken to be the θ-weighted average of the upper and lower surface values.

$$C_{\tau_{\text{wake}}} = \frac{C_{\tau_{\text{upper}}}\theta_{\text{upper}} + C_{\tau_{\text{lower}}}\theta_{\text{lower}}}{\theta_{\text{upper}} + \theta_{\text{lower}}} \qquad (18)$$

This gives the correct initial C_τ values for both a symmetrical case with identical upper and lower boundary layers, and also for a vastly asymmetrical case where one boundary layer completely dominates the wake and the other is largely irrelevant. The wake variables with their initial values defined above can be directly used in the governing equations (1),(2), (3), and the wake closure relations (13) - (15) to determine downstream wake development.

3 Blunt Trailing Edge Corrections

Initial calculations with the above formulation still gives unsatisfactory comparisons with the experimental C_p, δ^*, and θ distributions measured by Cook and McDonald [5]. The rapid C_p rise downstream of the trailing edge is underpredicted, which automatically underpredicts the θ rise via the momentum equation (1). Interestingly, the problem arises from the shape parameter correlation (6). This relation has been developed using Swafford's [8] velocity profile formula given below, which yields a profile very similar to the perhaps more familiar composite logarithmic wall layer plus Coles [10] half-sine outer layer representation.

$$\frac{u(\eta)}{u_e} = \sqrt{\frac{C_f}{2}}\,\frac{1}{0.09}\arctan\left[0.09\,\frac{\rho u_e \eta}{\mu}\sqrt{\frac{C_f}{2}}\right] + \left\{1 - \sqrt{\frac{C_f}{2}}\,\frac{\pi}{0.18}\right\}\tanh^{\frac{1}{2}}\left[a(\eta/\theta)^b\right] \qquad (19)$$

The constants a and b are implicitly determined by specifying kinematic momentum and displacement thicknesses. Specifying the experimental values measured by Cook and McDonald [5], using upper and lower wake values below and above the minimum velocity point, permits the direct comparison of Swafford's profile formula (19) and the experimental data as shown in Figure 3. On the airfoil surface, and in the far wake, this assumed profile family quite accurately represents the measured profiles. However, the representation is very poor in the near wake behind a blunt trailing edge due to the "dead air" region which cannot be accounted for in the simple two-layer profile model. Figure 4 shows the large resulting deviations from the $H^* - H_k$ correlation (6) calculated directly from Swafford's profile formula (19). This deviation creates large errors in $dH^*/d\xi$, which produces incorrect $du_e/d\xi$ and hence dC_p/dx levels via the shape parameter equation (2). This in turn gives the incorrect $d\theta/d\xi$ levels via the momentum equation (1) as noted earlier. Also, the dissipation coefficient C_D in general depends on the details of the velocity profile. A wrong assumed profile will lead to incorrect dissipation levels, which again will contribute to errors in $du_e/d\xi$ via the shape parameter equation (2).

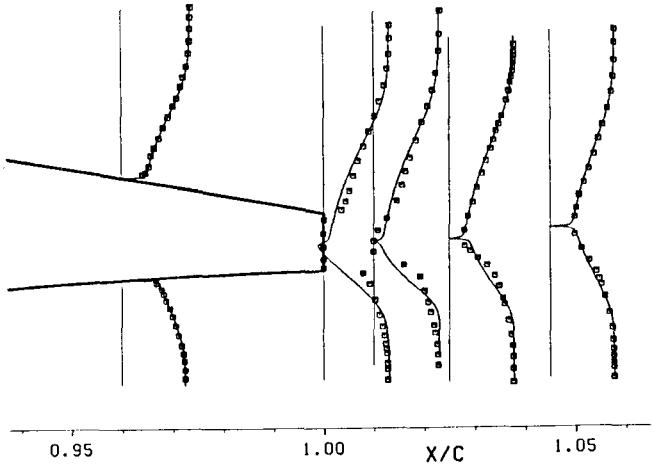

Figure 3: Assumed profiles (solid lines) based on measured (symbols) kinematic δ^* and θ from Case 3.

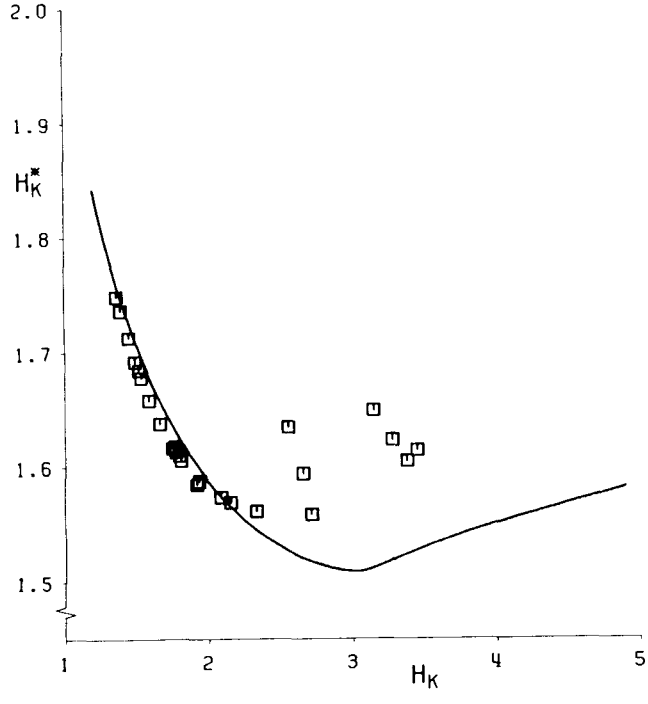

Figure 4: Assumed shape parameter correlation and experimental values (symbols) based on total wake profiles from Cases 1 - 4.

Simple corrections which largely eliminate these errors involve assuming a shape and length of the dead air region. As suggested by Cook and McDonald [5], a cubic distribution of the wake dead air width δ_w accurately models the observed flow. The present formulation uses the following shape.

$$\delta_w = h_{TE}\left\{1 + \left[2 + \frac{L_w}{h_{TE}}\frac{dt}{dx}\right]\bar{\xi}\right\}\left(1-\bar{\xi}\right)^2 \qquad (20)$$

where $\bar{\xi}$ is a non-dimensionalized distance from the trailing edge

$$\bar{\xi} = \frac{\xi - \xi_{TE}}{L_w} \quad ,$$

dt/dx is the airfoil thickness slope at the trailing edge (negative tangent of the trailing edge angle) , and L_w is the length of the dead air region, empirically taken to be

$$L_w = 2.5\, h_{TE} \qquad (21)$$

The dead air region shape matches the airfoil trailing edge angle and is cusped at its rearmost point, which purposely avoids outside and inside corners on the displacement body. Using the measured kinematic $(\delta^* - \delta_w)$ and θ values to determine the constants a and b in the profile formula (19) instead of just δ^* and θ, gives a much better fit to the assumed and experimental profiles as shown in Figure 5.

For computational purposes, the width δ_w of the dead air region is used to define a modified shape parameter

$$\tilde{H} = H - \frac{\delta_w}{\theta} \qquad (22)$$

which characterizes the wake velocity profiles with the dead air region excluded. $\tilde{H}$ is now used define all the subsequent quantities using the original functional expressions (5) - (9), and the quadrupled wake $C_{\tau_{EQ}}$ expression (13).

$$\tilde{H}_k = H_k(\tilde{H}, M_e) \qquad (23)$$

$$\tilde{H}^* = H^*(\tilde{H}_k, M_e, Re_\theta) \qquad (24)$$

$$\tilde{H}^{**} = H^{**}(\tilde{H}_k, M_e) \qquad (25)$$

$$\tilde{\delta} = \delta(\tilde{H}_k, \theta, (\delta^* - \delta_w)) \qquad (26)$$

$$\tilde{U}_S = U_S(\tilde{H}^*, \tilde{H}, \tilde{H}_k) \qquad (27)$$

$$\tilde{C}_{\tau_{EQ}} = 4\, C_{\tau_{EQ}}(\tilde{H}^*, \tilde{H}, \tilde{H}_k, \tilde{U}_S) \qquad (28)$$

At the programming level, this is a trivial change since only H needs to be redefined, and subsequent redefinitions follow automatically. The only place where the unmodified shape parameter H is always used is in the integral equations (1) and (2) themselves.

Replacing H_k with $\tilde{H}_k$ and H^* with $\tilde{H}^*$ in the kinetic energy shape parameter function (24) gives a much better correlation with experiment than the original $H^* - H_k$ function as shown in Figure 6. This is to be expected since the profile formula (19) is now fairly accurate as can be seen from Figure 5. The same replacement of H_k with $\tilde{H}_k$ is applied to the density thickness shape parameter function (25) although the available experimental data is insufficient

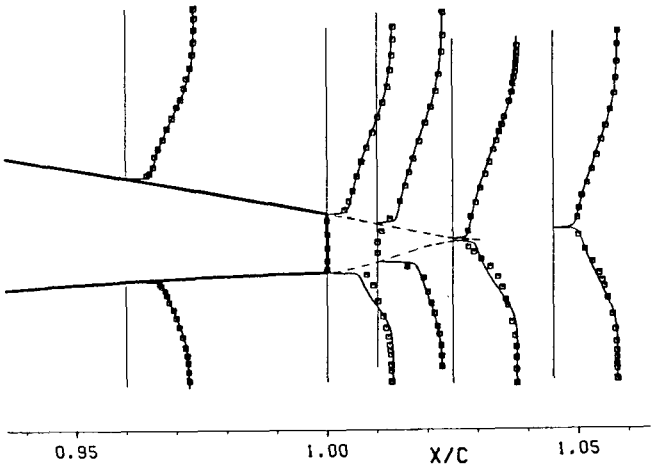

Figure 5: Assumed profiles (solid lines) based on measured (symbols) kinematic δ^* and θ from Case 3, excluding assumed dead air region.

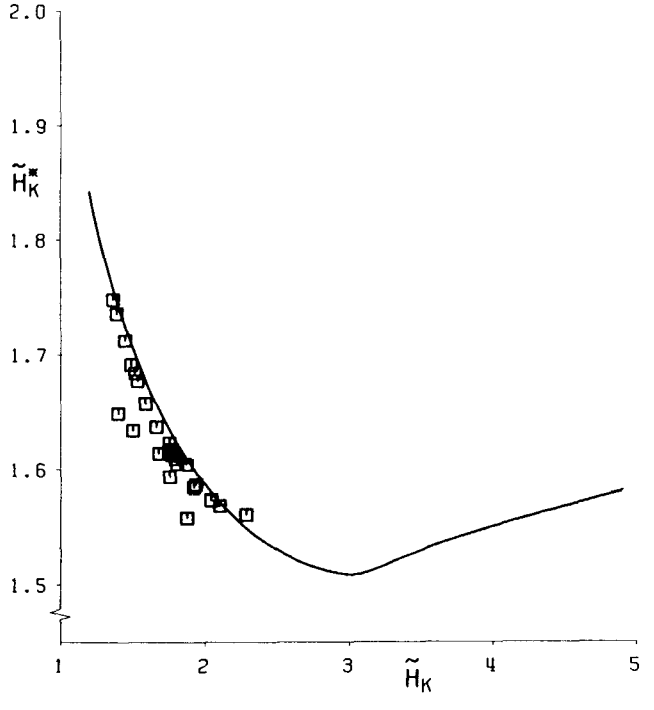

Figure 6: Assumed shape parameter correlation and experimental values (symbols) based on total wake profiles from Cases 1 - 4, excluding assumed dead air region.

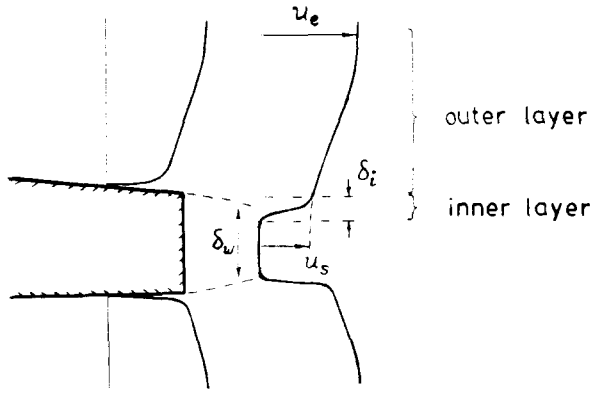

Figure 7: Outer and inner shear layers over dead air region.

to access the accuracy of this modification. The effect of H^{**} in the governing equations is quite small in any case. The other quantities are similarly modified, the test of their validity being the performance of the resulting calculation method.

An additional correction needs to be added to the total wake dissipation function (15) to account for the distorted profiles in the dead air region. In particular, there will be additional shear work in the steep shear layer between the dead air region and the outer layer, clearly visible in the experimental profiles shown in Figure 5. As sketched in Figure 7, the overall profile is composed of the usual outer layer and the steep inner shear layer, both of which appear to have the characteristic Coles [10] half-sine shape in the experimental profiles. If the inner layer has a thickness δ_i and the velocity jump across it is $u_S = u_e U_S$, or simply the slip velocity of the outer layer, the inner shear layer velocity profile can be written as follows.

$$\frac{u}{u_e} = \frac{U_S}{2}\left[1 - \cos \pi \frac{\eta}{\delta_i}\right] \tag{29}$$

Assuming that the turbulence in this inner shear layer behaves much like the turbulence in the outer layer, its Clauser [6] eddy viscosity is given by

$$\begin{aligned} \mu_t &= K \rho_e u_e \int_0^{\delta_i} \left(U_S - \frac{u}{u_e}\right) d\eta \\ &= K \rho_e u_e \frac{\delta_i}{2} U_S \end{aligned} \tag{30}$$

with $K \simeq 0.016$. The corresponding shear stress is then given by

$$\begin{aligned} \tau &= \mu_t \frac{\partial u}{\partial \eta} \\ &= \rho_e u_e^2 \frac{\delta_i}{2} U_S \frac{\partial (u/u_e)}{\partial \eta} \end{aligned} \tag{31}$$

and its additional shear work (dissipation) contribution can be determined.

$$C_{D_{\text{inner}}} \equiv \frac{1}{\rho_e u_e^3} \int_0^{U_S} \tau \, d\left(\frac{u}{u_e}\right) = K \frac{\pi^2}{16} U_S{}^3 \tag{32}$$

Because it is thin, the inner shear layer will reach some equilibrium turbulent state relatively quickly after the turbulence-inhibiting effect of the airfoil surface disappears (much faster than the thick outer layer). The Clauser eddy viscosity model above which assumes an equilibrium flow should then be reasonably accurate.

The above model for the additional dissipation due to the inner shear layer dictates that the contribution should be added as long as the thickness of the assumed dead air region is nonzero. However, examination of the experimental profiles in Figure 5 indicates that some merging of the two inner layers occurs before the end of the assumed dead air region, which reduces the velocity gradients and also the associated dissipation. To crudely model this effect and also to smoothly drop the additional dissipation contribution to zero as the dead air region closes up, the dissipation contribution given by equation (32) should be weighted by a factor which starts at unity at the airfoil trailinge edge and smoothly drops off to zero as the dead air region closes up. A convenient factor is simply the dead air thickness to trailing edge thickness ratio δ_w/h_{TE}.

$$C_D = 2\left[C_\tau(1-U_S) + K\frac{\pi^2}{16}U_S^3\frac{\delta_w}{h_{TE}}\right] \qquad (33)$$

where it is assumed that $\delta_w = 0$ after the dead air region disappears.

4 Results

4.1 RAE 2822 Airfoil Test Cases

Cook and McDonald [5] present four tests on a model of an RAE 2822 airfoil with the trailing edge truncated, leaving a 1.14% thick trailing edge with sharp corners. These four cases were computed using the ISES code with the new wake formulation. A standard 132×32 grid was used, with a somewhat finer than usual grid resolution in the trailing edge region, shown in Figure 8. The ISES code uses a streamline inviscid grid, and the streamwise boundary layer resolution is the same as that of the inviscid grid on the displacement streamline. The experiment had roughness strips at 3% chord, and hence transition was forced at 4% and 6% on the suction and pressure surfaces. Transition on the pressure surface is expected to be somewhat delayed due to the strongly favorable pressure gradient.

Figures 9 through 12 show the calculated C_p distributions for Cases 1 through 4 , together with the experimental C_p distributions. The predicted drag is noticably larger and more accurate than that from the original ISES formulation. The C_p gradient just past the trailing edge is somewhat overpredicted, but it must be realized that the experiment reports a measurable static pressure gradient across the wake in this region, leaving some amibiguity as to what is the appropriate pressure to compare against in the calculation. The experimental pressures shown in Figures 9 through 12 are taken from the point in the upper

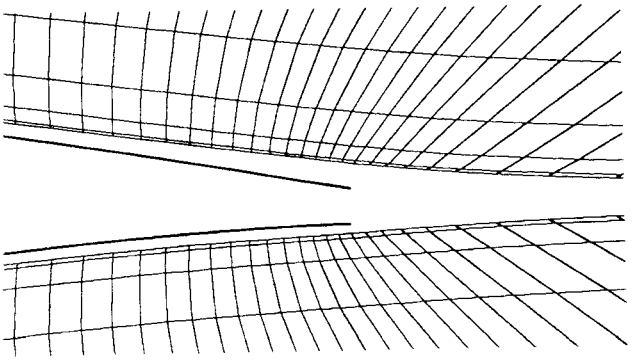

Figure 8: Inviscid grid in the trailing edge region.

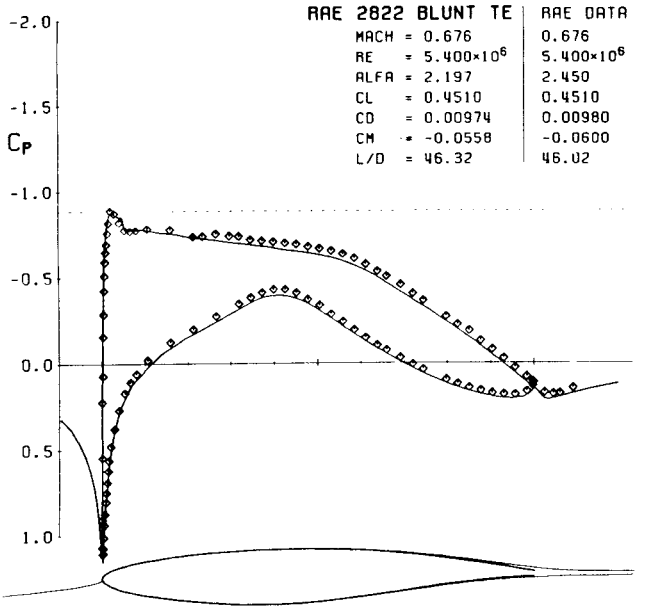

Figure 9: Case 1. Calculated (line) and experimental (symbols) C_p vs x/c.

half-wake where the velocity is roughly one half of the local edge velocity. The calculated pressures are taken from the streamline on the displacement surface.

The normal pressure gradients also tend to cast doubt on the validity of the basic boundary layer formulation in the trailing edge region, as well as the displacement body model for the viscous effects. Figures 13 through 16 show good agreement of the computed δ^* distributions with the experimental measurements. If the displacement body model were perfectly valid, this would automatically imply that the C_p distributions must be predicted accurately also. The fact that the δ^* distributions are predicted very well the predicted C_p distributions are only fair, indicates that the validity of the displacement body modeling concept is beginning to break down for these cases. This perhaps is not too surprising since the displacement thickness is changing so rapidly in the near wake region. Short of a complete Navier-Stokes formulation for this problem which is presently unfeasible for a fast design tool such as ISES,

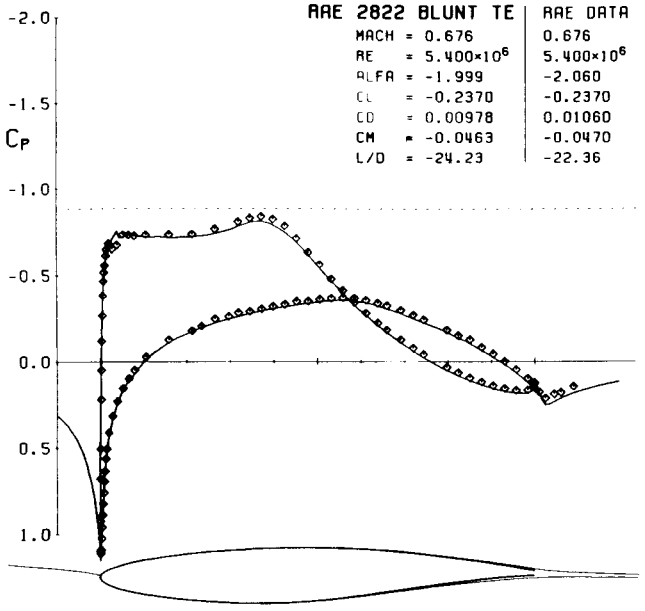

Figure 10: Case 2. Calculated (line) and experimental (symbols) C_p vs x/c.

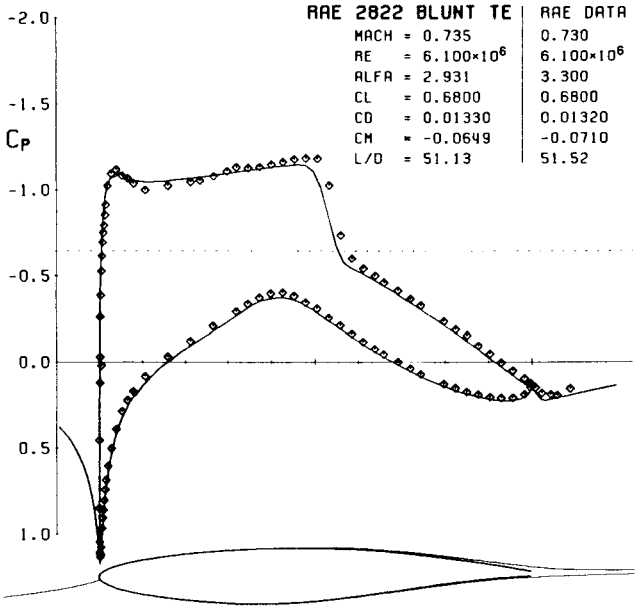

Figure 11: Case 3. Calculated (line) and experimental (symbols) C_p vs x/c.

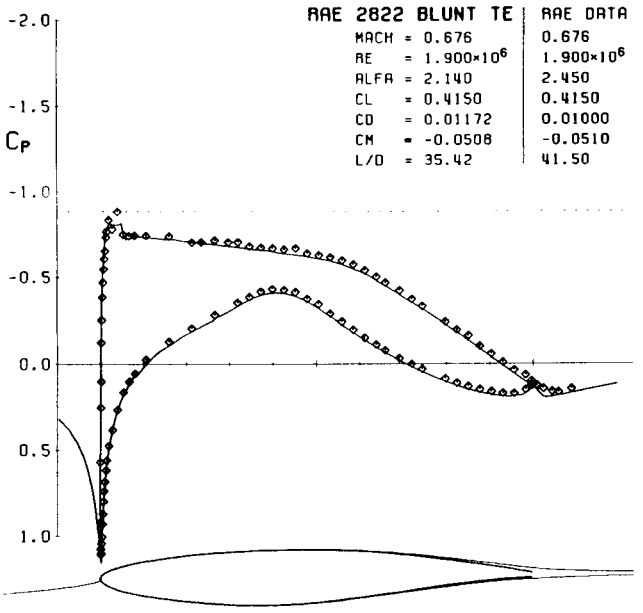

Figure 12: Case 4. Calculated (line) and experimental (symbols) C_p vs x/c.

some sort of correction for the normal pressure gradients would improve the C_p discrepancy. Unfortunately, no such corrections for integral methods exist at present. For design purposes, this shortcoming may be a moot point, however. It is more important for a viscous airfoil calculation method to predict the overall growth of the boundary layer and hence the drag, than the local C_p details. In this respect, the present approach performs quite well. The overall agreement of the δ^* and θ distributions shown in Figures 13 through 16 is very good, showing a marked improvement over the old calculated distributions for Case 1 in Figure 2.

4.2 Compressor Cascade Test Case

Hobbs et al [11] report an experiment involving measurements in the near-wake region of a transonic compressor cascade. The experiment itself was performed at a subcritical inlet Mach number of 0.1132 and a rather low chord Reynolds number of 480 000. Although the experiment report [11] provides a detailed account of all the test and geometric parameters, it does not provide the actual airfoil coordinates. These were generated from the reported experimental C_p distributions using the ISES design mode. The reported C_p was matched as closely as possible as shown in Figure 17, and the reported trailing edge thickness of 1.84% of the axial chord was matched exactly. The actual trailing edge in the experiment is semicircular, but this was modeled as being cut off flat as in the RAE 2822 airfoil cases. The separation off the rounded trailing edge is immediate so the geometric details should have little effect.

Figure 18 shows the calculated and experimental δ^* and

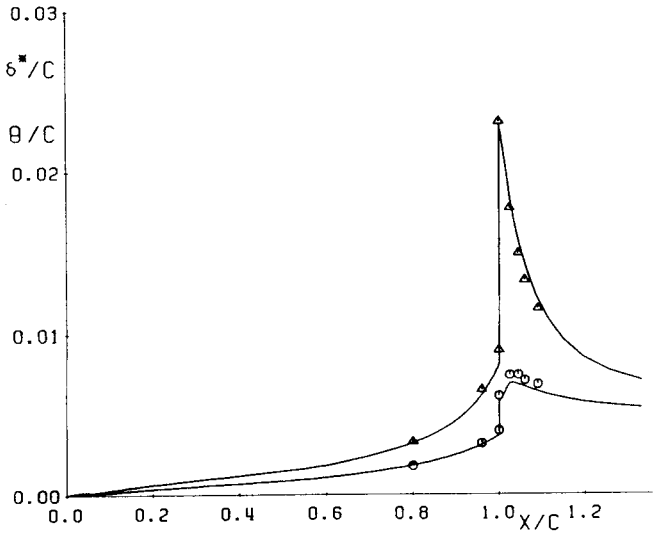

Figure 13: Calculated (line) and experimental (symbols) δ^* and θ vs x/c for Case 1.

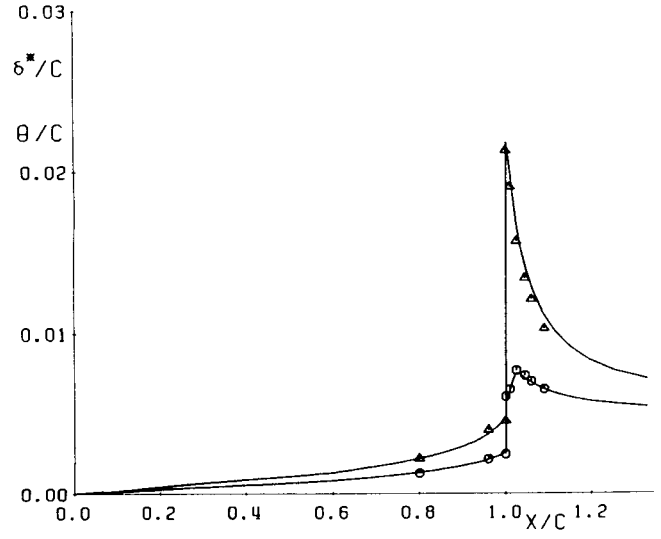

Figure 14: Calculated (line) and experimental (symbols) δ^* and θ vs x/c for Case 2.

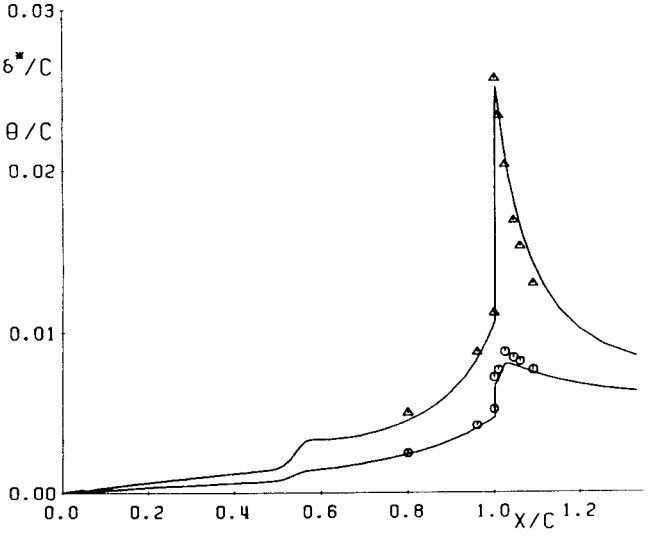

Figure 15: Calculated (line) and experimental (symbols) δ^* and θ vs x/c for Case 3.

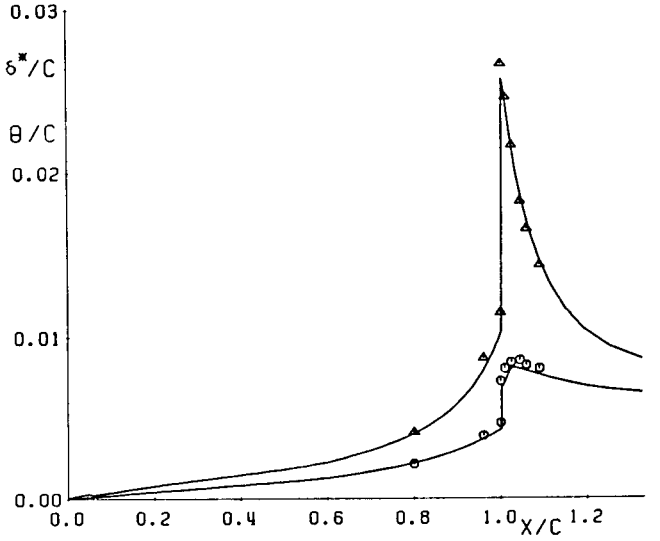

Figure 16: Calculated (line) and experimental (symbols) δ^* and θ vs x/c for Case 4.

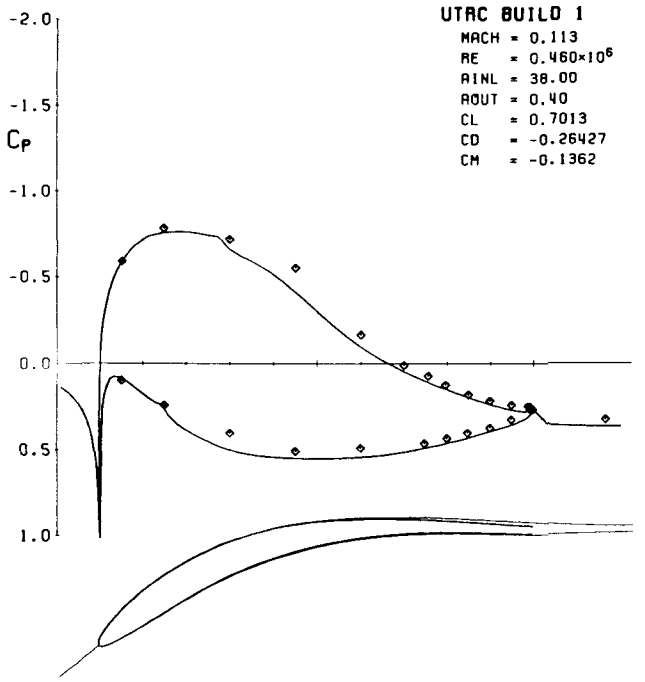

Figure 17: Calculated (line) and experimental (symbols) C_p vs x/c for compressor cascade.

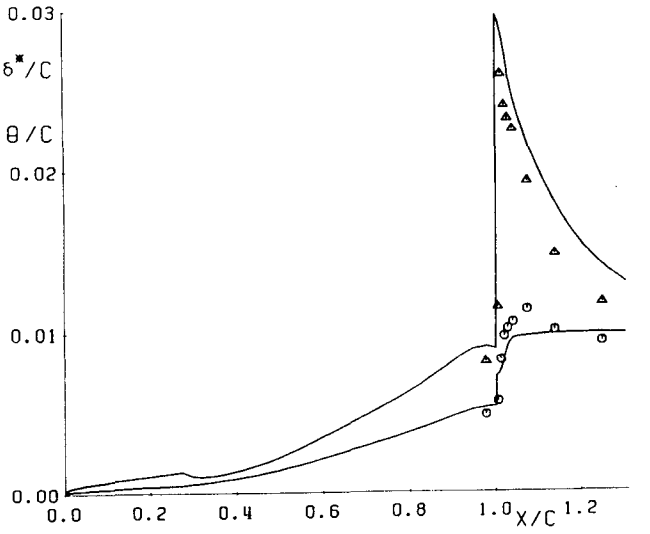

Figure 18: Calculated (line) and experimental (symbols) δ^* and θ vs x/c for compressor cascade.

θ distributions for the suction side and wake. Both the rate of decrease of δ^* and rate of increase of θ are underpredicted. It is believed that these discrepancies are the result of the von Karman type vortex shedding off the blunt trailing edge which was observed in the experiment. Although one can still fairly rigorously describe such a wake in the Reynolds-averaged sense, clearly the presence of the von Karman vortex street will change the fluctuating velocities u' and v' from their usual "steady" wake values. The apparent Reynolds stress $\overline{u'v'}$ will thus likely increase, raising the dissipation level in the process. To crudely test this hypothesis, a calculation was performed with the total dissipation in the wake rather arbitrarily doubled from the value given by expression (33).

$$C_D = 4\left[C_\tau(1-U_S) + K\frac{\pi^2}{16}U_S^3\frac{\delta_w}{h_{TE}}\right] \qquad (34)$$

As can be seen in Figure 19, the agreement is now somewhat better. Clearly more work is needed to properly quantify the effects of vortex shedding on the integral boundary layer parameters, particularly the dissipation levels. This is more important in turbomachinery than isolated airfoil applications. Turbomachinery blading frequently has relatively thick trailing edges, which is a key parameter in whether vortex shedding will occur. Reference [11] also reports the test of another compressor cascade with a much smaller 0.59% trailing edge thickness (versus 1.84%) which did not experience noticable vortex shedding.

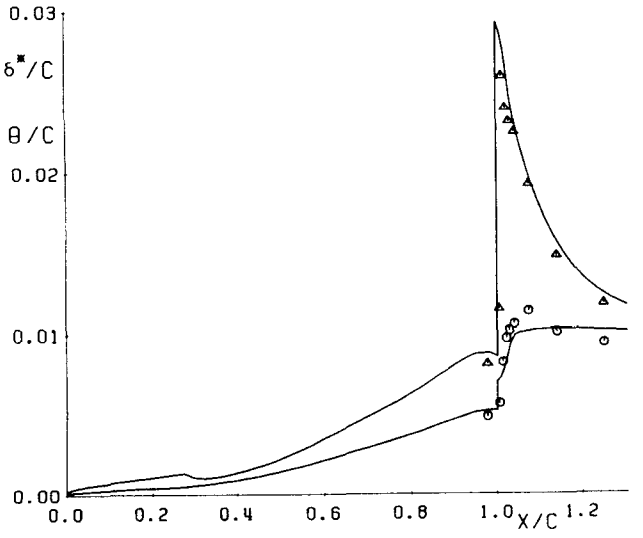

Figure 19: Calculated (line) and experimental (symbols) δ^* and θ vs x/c for compressor cascade with doubled dissipation coefficient in wake.

5 Conclusions

A modification to an existing integral boundary layer formulation has been developed to enable accurate prediction of the near-wake flow behind a blunt airfoil trailing edge. The rapid rise in momentum thickness and hence overall drag is particularly well predicted for several airfoil cases. The correction is relatively simple, and is applicable to all two-equation integral methods. Further work needs to be done for airfoil flows with periodic vortex shedding.

Acknowledgements

This research was supported by the MIT Carl Richard Souderton Faculty Development Chair.

References

[1] Drela,M., "Two-Dimensional Transonic aerodynamic Design and Analysis Using the Euler Equations," MIT Gas Turbine & Plasma Dynamics Laboratory Report No. 187, February 1986.

[2] Drela,M., Giles,M.B., "Viscous-Inviscid Analysis of Transonic and Low Reynolds Number Airfoils", AIAA Journal, Vol. 25, No. 10, October 1987.

[3] Drela,M., Giles,M.B., "ISES: A Two-Dimensional Viscous Aerodynamic Design and Analysis Code," AIAA Paper 87-0424, January 1987.

[4] Green,J.E., Weeks, D.J., Brooman, J.W.F. "Prediction of Turbulent Boundary Layers and Wakes in Compressible Flow by a Lag-Entrainment Method," ARC R&M Report No. 3791, HMSO, London, 1977.

[5] Cook,P.H., McDonald,M.A. "Wind Tunnel Measurements in the Boundary Layer and Wake of an Airfoil with a Blunt Base at high Subsonic Speeds," RAE Technical Report 84002, January 1984.

[6] Clauser,F.H., "Turbulent Boundary Layers in Adverse Pressure Gradients", Journal of Aeronautical Sciences, Vol. 21, No. 2, pp 91-108, February 1954.

[7] Narasimha,R., Prabhu,A., "Equilibrium and Relaxation in Turbulent Wakes", Journal of Fluid Mechanics, Vol. 54, Part 1, pp. 1-18, 1972.

[8] Swafford,T.W., "Analytical Approximation of Two-Dimensional Separated Turbulent Boundary-Layer Velocity Profiles," *AIAA Journal*, Vol. 21, No. 6, pp 923-926.

[9] Coles,D.E., "The Law of the Wake in the Turbulent Boundary Layer," Journal of Fluid Mechanics, Vol. 1, part 2, pp. 193-226, 1956.

[10] Hobbs,D.E., Wagner,J.H., Dannenhoffer,J.F., Dring,R.P., "Wake Experiments and Modeling for Fore- and Aft-Loaded Compressor Cascades," Pratt and Whitney Supercritical Airfoil Technology Program Report No. FR-13514, September 1980.